Chemical Geology 703 (2026) 123230

Contents lists available at ScienceDirect

Chemical Geology

journal homepage: www.elsevier.com/locate/chemgeo

Research Paper

Calcite TLM as a new natural reference material for in situ U-Pb geochronology and its geological implications

Tianyi Li [a,1], Ranran Chen [b,c,1], Shitou Wu [b,c,*], Rolf L. Romer [d], Nick M.W. Roberts [e], Kerstin Drost [f], David Chew [f], Marcel Guillong [g], Qian Ma [h], Yahui Yue [i], Shuangjian Li [a], Bohang Xie [b,c], Ahmatjan Abdurahman [a], Hao Wang [b,c], Huixi Lin [a], Yueheng Yang [b,c], Xusheng Guo [a]

[a] State Key Laboratory of Shale Oil and Gas Enrichment Mechanisms and Effective Development, Research Institute of Petroleum Exploration & Production, Sinopec, Beijing 100083, PR China
[b] State Key Laboratory of Lithospheric and Environmental Coevolution, Institute of Geology and Geophysics, Chinese Academy of Sciences, Beijing 100029, PR China
[c] College of Earth and Planetary Science, University of Chinese Academy of Sciences, Beijing 100049, PR China
[d] GFZ Helmholtz Centre for Geosciences, Telegrafenberg, D-14473 Potsdam, Germany
[e] Geochronology and Tracers Facility, British Geological Survey, Environmental Science Centre, Nottingham NG12 5GG, UK
[f] Discipline of Geology, School of Natural Sciences, Trinity College Dublin, Dublin 2, Ireland
[g] Department of Earth and Planetary Sciences, ETH Zürich, 8092 Zurich, Switzerland
[h] Institute of Geology, Chinese Academy of Geological Sciences, Beijing 100037, PR China
[i] Institute of Tibetan Plateau Research, Chinese Academy of Sciences, Beijing 100101, PR China

ARTICLE INFO

Editor: Sonja Aulbach

Keywords:
Calcite U-Pb geochronology
Reference materials
LA-ICP-MS
In situ microanalysis
Karstification

ABSTRACT

Calcite ($CaCO_3$) forms in a wide variety of geological environments as both a primary and secondary mineral phase and may contain sufficient U for U-Pb geochronology. The limited availability of well-characterized calcite reference materials, however, has impeded its broader application in microanalysis. In this study, a natural calcite sample (TLM) was characterized and assessed as a potential primary reference material for in situ U-Pb geochronology. U-Pb isotopic analyses were conducted across nine independent laboratories using laser ablation (Q, SF, MC)-ICP-MS and isotope dilution (ID)-TIMS, to examine the homogeneity and to determine the U-Pb age of TLM. Calcite TLM has an age homogeneity at the level of ~ 1.0 %, as indicated by multiple analyses from different laboratories. ID-TIMS analysis of 14 aliquots yielded an intercept age of 222.5 ± 2.8 Ma (2 s) with an initial $^{207}Pb/^{206}Pb$ value of 0.8380 ± 0.0013. Calcite TLM has an age uncertainty of 1.28 %, which is considerably lower than that of WC-1 (~2.5 %). Calcite TLM has U and Pb contents of ~0.35 μg g^{-1} and ~ 0.02 μg g^{-1}. Additional C and O stable isotope, radiogenic Sr isotope and trace element compositional data indicate that calcite TLM is likely sourced from meteoric water and indicate that the recurrent karstification may have affected the studied area as late as the Triassic.

1. Introduction

Calcite ($CaCO_3$) forms in a wide variety of geological settings as both a primary and secondary mineral phase, including diagenetic, biogenic, igneous, metamorphic, and hydrothermal environments (Roberts et al., 2020). Calcite can potentially incorporate sufficient U for U-Pb geochronology (Coogan et al., 2016; Moorbath et al., 1987; Roberts and Walker, 2016; Smith et al., 1991). Pb-Pb dating of calcite has been undertaken for nearly four decades (Moorbath et al., 1987), and was followed by U-Pb dating of carbonate diagenesis (Smith et al., 1991). Both isotope dilution thermal ionization mass spectrometry (TIMS) and multiple collector inductively coupled plasma mass spectrometry (MC-ICP-MS) were initially used for calcite U-Pb dating (Mason et al., 2013; Moorbath et al., 1987; Smith et al., 1991; Woodhead et al., 2006; Woodhead and Pickering, 2012). However, the time-consuming nature of such solution-based laboratory work (dissolution and column-

* Corresponding author.
E-mail address: shitou.wu@mail.iggcas.ac.cn (S. Wu).
[1] These authors contributed equally: Tianyi Li, Ranran Chen.

https://doi.org/10.1016/j.chemgeo.2025.123230
Received 21 October 2025; Received in revised form 27 December 2025; Accepted 27 December 2025
Available online 29 December 2025

chemistry) and the resultant low sample throughput mean that limited amounts of data were generated from these approaches (Rasbury and Cole, 2009). Since the first attempt for calcite U-Pb dating using laser ablation (LA) ICP-MS in the 2010s (e.g., Li et al., 2014), substantially more datasets have been generated resulting in a big step forward in this field (Coogan et al., 2016; Roberts et al., 2020; Roberts and Walker, 2016). Compared with isotope dilution methods, LA-ICP-MS has the advantages of high spatial resolution, rapid analysis (less than two

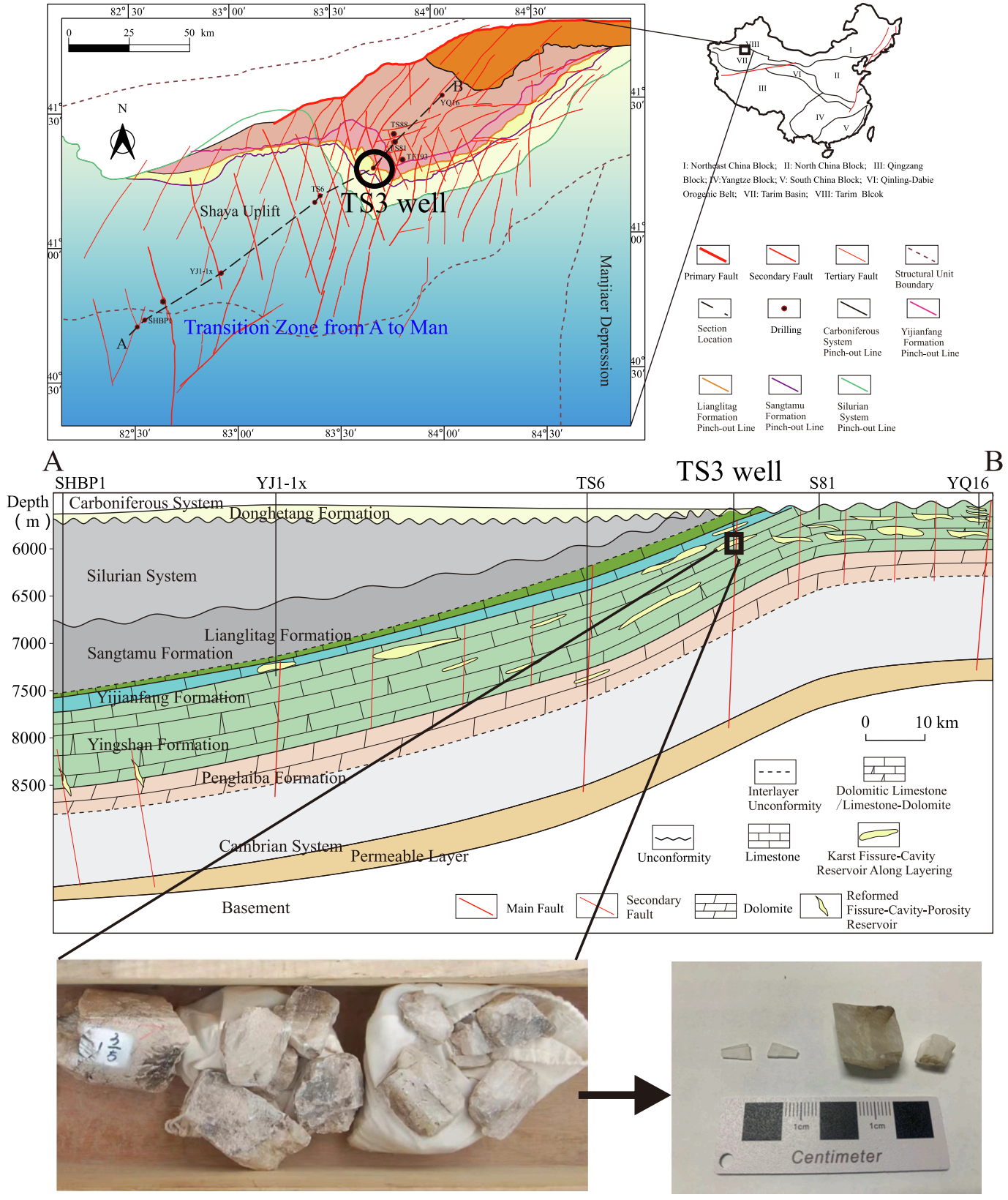

Fig. 1. Structural and stratigraphic map for the TS3 Well and its surrounding region, and the photograph of specimen and crushed fragments of calcite TLM.

minute per spot analysis) and an ability to collect a wide spread in U/Pb ratio yielding better constrained isochron / intercept ages (Roberts et al., 2020).

Recently, the further improvement of instrument sensitivity using sector field (SF) single collector or multiple collector ICP-MS (Guillong et al., 2020; Wu et al., 2022; Xie et al., 2023; Yokoyama et al., 2018; Zhang et al., 2021) along with imaging-guided and/or imaging-based techniques have improved the applications of the method (Drost et al., 2018; Gui et al., 2025; Hoareau et al., 2021; Roberts et al., 2020). The LA-ICP-MS approach is now widely used (Roberts et al., 2020), but importantly it requires matrix-matched reference materials to correct for mass bias of U/Pb ratio and to monitor the data accuracy. Compared to LA-ICP-MS dating of zircon, which has >20 well characterized reference materials, there is a lack of calcite reference materials for U-Pb dating which yield non-dispersed and sufficiently radiogenic U/Pb data. Currently, there are several reference materials characterized by isotope dilution (ID) technique, including WC-1(Roberts et al., 2017), Duff Brown Tank (Hill et al., 2016), ASH-15D (Nuriel et al., 2020), JT (Guillong et al., 2020), RA138 (Guillong et al., 2024), TARIM (Zhang et al., 2023a), PTKD-2 (Nguyen et al., 2019), SB19 (Wang et al., 2025), and RioM-1(Silva et al., 2025). In addition to these, some laboratories use in-house reference materials only characterized by LA-ICP-MS, such as B6 (Pagel et al., 2018), AHX-1D (Cheng et al., 2020), LD-1 (Kendrick et al., 2022), and DC22 (Tang et al., 2025).

Among them, WC-1 is widely used as the primary reference material for calcite U-Pb dating (Roberts et al., 2017), but it has a relatively large age uncertainty of ~2.5 % which propagates through to unknown samples with a resultant total uncertainty of at least ~3.0 %. In this study, we investigated a low common Pb calcite from the Ordovician Yingshan Formation of Well TS3 in the Tarim Basin, China. The homogeneity of this new calcite reference material (TLM) was evaluated using multiple spot analyses in a single laboratory and subsequently cross-checked by seven other independent LA-ICP-MS laboratories. The recommended U-Pb age for TLM was obtained using ID-TIMS analysis. To constrain the petrogenesis of the sample, we also acquired C and O stable isotope data as well as trace element compositional data and integrated them with the published radiogenic Sr isotope data (Wu et al., 2023).

2. Sample description and geological background

The sample was obtained from Well TS3 in the Ordovician Yingshan Formation in the Tarim Basin, at a sampling depth of 6104.6 m (Fig. 1a, b). The Yingshan Formation was formed in an open platform sedimentary environment, with localized development of inner-platform shoals and patch reefs. Water depth increased to the south transitioning from grey to greyish-yellow sparry grainstone and mud-grain limestone on the shallow open platform to dark grey mud-grain limestone and grain-mud limestone on the deeper open platform. In the Well TS3, the formation primarily is comprised of dolomitic limestone, micritic limestone, micritic grainstones and grainstones, with localized stratiform karst development and c. 6.81 m thick open space now filled by calcite.

Karstification in the region is related to prolonged (>100 Ma) exposure, erosion, and modification by meteoric freshwater (Mendez et al., 2020; Zhang and Cai, 2007). Extensive drilling and seismic surveys show that karstification has resulted in the development of multiple fracture-cavity reservoirs within 200 m beneath the Silurian unconformity (Tian et al., 2019; You et al., 2023). The fracture systems in the study area have been reactivated multiple times from the later Ordovician to the Triassic. About 30 g TLM samples were investigated in this study; parts of them were already used as an in-house calcite Sr isotope reference material at the Institute of Geology and Geophysics, Chinese Academy of Sciences (IGGCAS) (Wu et al., 2023). The entire crystal was broken up, including the inner portions and the rim. Fifty chips were set aside for distribution to the analytical community and the others were preserved for future usage. Calcite TLM has a U concentration of ~0.35 μg g^{-1}.

3. Analytical techniques

Nine laboratories from eight institutions were participated in this study. They are the Institute of Geology and Geophysics, Chinese Academy of Sciences, Beijing, PR China (IGGCAS), Research Institute of Petroleum Exploration & Production, Sinopec, Beijing, PR China (PP). Helmholtz Centre for Geosciences, Potsdam, Germany (GFZ), Department of Earth and Planetary Sciences, ETH Zürich, Switzerland (ETH), Geochronology and Tracers Facility, British Geological Survey, Environmental Science Centre, Nottingham, UK (BGS), iCRAGLab@TCD/Centre for Microscopy & Analysis, Trinity College Dublin, Dublin, Ireland (TCD), Institute of Geology, Chinese Academy of Geological Sciences, Beijing, PR China (CAGS), Institute of Tibetan Plateau Research, Chinese Academy of Science, Beijing, PR China (ITPRCAS). The analytical techniques employed include cathodoluminescence (CL), LA-(Q, SF, MC)-ICP-MS and ID-TIMS. Table 1 summarizes the elements measured, the number of samples analyzed, the analytical techniques and the institutions that carried out the analyses. Key features of the analytical techniques used for characterization are summarized in Table 1 and are described below.

3.1. Cathodoluminescence imaging

The cathodoluminescence (CL) imagery was undertaken at the Sinopec Petroleum Exploration and Development Research Institute using a CLF-2 cathodoluminescence system (Beacon Innovation International) and a Leica DM4500 P microscope. Polished sample mounts were not carbon-coated before CL imaging. An acceleration voltage of 18.8 kV and beam current of 0.434 μA were used.

3.2. Chemical analysis by LA–ICP–MS

The chemical compositions of TLM were determined by LA–ICP–MS using a 193 nm ArF excimer LA system (GeoLas HD, Lambda Physik, Göttingen, Germany) coupled to an Element XR HR-ICP-MS instrument (Thermo Fisher Scientific, USA) at the Institute of Geology and Geophysics, Chinese Academic of Sciences, Beijing, China. The analytical approach was similar to that outlined by Wu et al. (2018) and used a laser spot diameter of 44 μm, ablation frequency of 5 Hz, and laser energy density of ~4.0 J cm^{-2}. Helium was used as the ablation gas to improve the transport efficiency of the ablated aerosols. The ARM-1 glass reference material (Wu et al., 2019) was used to calibrate elemental concentrations, and NIST SRM 610 (Jochum et al., 2011) and BCR-2G (Jochum et al., 2005) were analyzed for quality control purpose. The specific elements and their dwell times are listed in ESI Table S1. Data reduction was performed using the Iolite 3.7 software with the bulk carbonate compounds (XCO_3, X represent the metal elements) normalized to 100 % to correct for the variations in ablation yields. For most trace elements (>0.05 μg g^{-1}), the analytical accuracy was better than ±10 % (one relative deviation) and the precision was better than ±10 % (one relative standard deviation) based on the NIST SRM 610 and BCR-2G data in ESI Table S2.

3.3. LA-ICP-MS U-Pb geochronology

Fragments of calcite TLM were picked randomly from the broken crystals and distributed to the nine laboratories for analysis. Three laboratories carried out U-Pb analyses using Q-ICP-MS (TCD, ITPCAS and CAGS). Four laboratories carried out U-Pb analyses using SF-ICP-MS (IGGCAS, PP, ETH and BGS). A single laboratory carried out U-Pb analyses using MC-ICP-MS at IGGCAS (Table 1). All laboratories used NIST614 or ARM-3 glass as calibration standards and the calcite WC-1 reference material for matrix-matching of the $^{238}U/^{206}Pb$ ratio. The final ages are given as "age ± a/b", where "a" is the uncertainty derived from regression of the data points and "b" is propagated to include systematic uncertainties (2.5 %). Any data outliers were rejected if they

Table 1
Summaries of the institute, instrumentation, measured isotopes, reference materials, and calibration procedures for the LA-ICP-MS U-Pb geochronology.

Institute	IGGCAS1	IGGCAS2	PP	ETH	BGS	TCD	ITPRCAS	CAGS
LA instrument	Geolas HD	Analyte G2	Newwave 213	Resolution S155	New Wave NWR 193^{UC}	Teledyne/ PhotonMachines Iridia	New Wave HE	New Wave NWR 193^{UC}
Laser source	CompexPro 193 nm	ATL	Tempest 213	CompexPro 193 nm	ATL	MLaser MLI 500 ArF LC (H)	CompexPro 193 nm	ATL
Pulse width	~ 20 ns	< 4 ns	~5 ns	~ 20 ns	< 4 ns	~ 5 ns	~ 20 ns	< 4 ns
Fluence on sample (J cm^{-2})	~ 2.0	~ 2.0	~3	~ 2.0	3.5-4.0	~ 2.2	~ 5.0	~ 3.0
Beam diameter	90 μm circle	85 μm circle	100 μm circle	110 μm circle	80 μm circle	80 μm square	150 μm circle	150 μm circle
Repetition rate	10 Hz	10 Hz	10 Hz	5 Hz	10 Hz	65 Hz	10 Hz	10 Hz
Ablation Cell	In-house built low-dispersion cell	HelEx II ablation cell	TV1	Laurin Technic S-155	TV2	Cobalt low-dispersion cell	TV3	TV2
Smoothing device	"Wave" signal-smoothing and Mercury removing device	"Wave" signal-smoothing and Mercury removing device	None	Squid from Laurin Technic	None	None	None	None
ICPinstrument	Element XR	Neptune Plus	Element II	Element XR	Nu Attom	Agilent 7900	Agilent 7900	Agilent 7900
Sample cone	Jet-version	Jet-version	Standard	Jet-version	–	Ni	Ni	Ni
Skimmer cone	H-version	X-version	H-version	H-version	–	Ni (for use with x-lens)	Ni	Ni
Mass resolution	~300	~300	~300	~300	~300	~300	~300	~300
Typical sensitivity	0.80 %	1.50 %	0.5 %	1.00 %	0.80 %	0.2–0.3 %	0.2–0.3 %	0.10 %
Oxide formation rate (ThO^+/Th^+)	< 0.3 %	< 0.3 %	< 1.0 %	< 0.2 %	< 0.2 %	< 0.2 %	< 0.3 %	0.08 %
detector mode	Triple (counting, analogue and Faraday)	IC and Faraday	Pulse/ analogue	Pulse/analogue	Pulse/ analogue	Pulse/analogue	Pulse/analogue	Pulse/analogue
Isotopes and/ or dwell time [ms]	^{202}Hg[2], ^{204}Hg + Pb[2], ^{206}Pb[15], ^{207}Pb[30], ^{208}Pb[2], ^{232}Th[2], ^{238}U[10]	^{202}Hg[13], ^{204}Hg + Pb[13], ^{206}Pb[13], ^{207}Pb[13], ^{208} Pb[13], ^{232}Th[13], ^{238}U[13]	^{202}Hg[2], ^{204}Hg + Pb[2], ^{206}Pb[15], ^{207}Pb[30], ^{208} Pb[2], ^{232}Th[2], ^{238}U[10]	^{202}Hg[11], ^{204}Hg + Pb[11], ^{206}Pb[50], ^{207}Pb[50], ^{208} Pb[11], ^{232}Th[11], ^{238}U[11]	^{202}Hg, ^{204}Hg + Pb, ^{206}Pb, ^{207}Pb, ^{208} Pb, ^{232}Th, ^{238}U	^{25}Mg[3], ^{43}Ca[5], ^{51}V[3], ^{55}Mn[3], ^{57}Fe[3], ^{63}Cu[3], ^{66}Zn[4], ^{71}Ga[4], ^{85}Rb[4], ^{88}Sr[2], ^{137}Ba[2], ^{140}Ce[2], ^{202}Hg[1], ^{204}Hg + Pb[1], ^{206}Pb[40], ^{207}Pb[100], ^{208}Pb[40], ^{232}Th[15], ^{238}U[25]	^{202}Hg[10], ^{204}Hg + Pb[10], ^{206}Pb[15], ^{207}Pb[30], ^{208} Pb[15], ^{232}Th[10], ^{238}U[10]	^{202}Hg[10], ^{204}Hg + Pb[10], ^{206}Pb[15], ^{207}Pb[30], ^{208} Pb[15], ^{232}Th[10], ^{238}U[10]
U/Th ratios on reference materials	1.0–1.1 on NIST SRM 612	1.0–1.1 on NIST SRM 612	1.0–1.1 on NIST SRM 612	1.0–1.1 on NIST SRM 612	1.0–1.1 on NIST SRM 612	1.0–1.1 on NIST SRM 612	1.0–1.1 on NIST SRM 612	1.0–1.1 on NIST SRM 612
Calibration reference material	NIST 614/ ARM-3 for ^{207}Pb/^{206}Pb WC-1 for ^{238}U/^{206}Pb	NIST 614/ ARM-3 for ^{207}Pb/^{206}Pb WC-1 for ^{238}U/^{206}Pb	NIST 614for ^{207}Pb/^{206}Pb WC-1 for ^{238}U/^{206}Pb	NIST 614 for ^{207}Pb/^{206}Pb WC-1 for ^{238}U/^{206}Pb	NIST 614/ ARM-3 for ^{207}Pb/^{206}Pb WC-1 for ^{238}U/^{206}Pb	NIST SRM 614 for ^{207}Pb/^{206}Pb WC-1 for ^{238}U/^{206}Pb	NIST 614/ ARM-3 for ^{207}Pb/^{206}Pb WC-1 for ^{238}U/^{206}Pb	NIST 614/ ARM-3 for ^{207}Pb/^{206}Pb WC-1 for ^{238}U/^{206}Pb
Software	Iolite 3.7	Iolite 3.7	Glitter	Iolite 4.0	Iolite 3.7	Iolite 3.7	Iolite 3.7	Iolite 4.0
Quality control material	Duff Brown Tank	ASH-15D and JT	–	JT, ASH-15D, B6, RA138	ASH-15D and B6	Duff Brown Tank	TARIM	Duff Brown Tank

Note: The typical sensitivity refers to ions detected/atoms sampled *100 as suggested by Horstwood et al. (2016).

clearly fall off the isochron, and this criterion were used consistently across all laboratories. The individual TLM data and the quality control material data are listed in ESI Table S3 and Table S4.

At TCD, U-Pb and trace element mapping was carried out using an Agilent 7900 quadrupole ICP-MS coupled to a Teledyne/PhotonMachines Iridia 193 nm Excimer laser system. The general analytical protocol and data processing follows Drost et al. (2018), while specific instrument settings and operating conditions are given in Table 1. NIST SRM 614 glass was used as the primary reference material, and calcite WC-1 was analyzed for matrix-matching of the $^{238}U/^{206}Pb$ ratio, and Duff Brown Tank limestone as quality control (Hill et al., 2016). Laser sampling employed a fluence of 2.2 J cm^{-2}, 80 μm square spots, a repetition rate of 65 Hz, and a scan speed of 30 μm s^{-1}. Data processing was done in Iolite v3.7 (Chew et al., 2014; Paton et al., 2011; Petrus and Kamber, 2012) with the Monocle add-on (Petrus et al., 2017) and an in-house spreadsheet. Calcite TLM was analyzed along 20 linear rasters of 74 s duration each resulting in c. 25 min of total signal compiled into W 2211 × H 1600 μm element and isotope ratio maps with 980 pixels. Pixel data were filtered (Ca > 35 wt%, $^{208}Pb > 0$ cps, $^{207}Pb > 70$ cps; 841 of 980 pixels used for U/Pb geochronology) and pooled into pseudo-analyses ($n = 40$ comprising c. 30 s of signal / c. 20 pixels each) using the empirical cumulative distribution function of the $^{207}Pb/^{235}U$ channel.

At ITPCAS, U-Pb analyses by LA-ICP-MS utilized an Agilent 7900 ICP-MS coupled to a New Wave Research (ESI) NWR193HE laser ablation system equipped with a TV3 ablation cell. Laser ablation parameters for carbonates are a spot size of 150 μm, ablation frequency of 10 Hz and a fluence of 3–4 J cm^{-2}. WC-1 was used as primary calibration material (Roberts et al., 2017). TARIM was analyzed as quality control material (Zhang et al., 2023a). NIST SRM 614 was first used as the reference material to correct for instrument drift and to correct the isotopic ratio of $^{207}Pb/^{206}Pb$ and $^{238}U/^{206}Pb$, and subsequently WC-1 was used to correct the matrix bias of $^{238}U/^{206}Pb$ ratio, as described by Roberts et al. (2017). Intercept ages were calculated using IsoplotR

(Vermeesch, 2018). A total of 27 spot analyses were made.

At CAGS, the experiment was carried out with an Agilent 7900 ICP-MS coupled to a New Wave Research (ESI) NWR193UC laser ablation system equipped with a TV2 ablation cell. Laser ablation parameters for calcite dating are a spot size of 150 μm, ablation frequency of 10 Hz and a fluence of ~3.0 J cm^{-2}. The data reduction method largely follows those of Hansman et al. (2018), Nuriel et al. (2020), Ring and Gerdes (2016) and Roberts et al. (2017). NIST SRM 614 was first used as the reference material to correct for instrument drift and to correct the isotopic ratio of $^{207}Pb/^{206}Pb$ and $^{238}U/^{206}Pb$, and subsequently WC-1 was used to correct the matrix bias of $^{238}U/^{206}Pb$ ratio. Duff Brown Tank was analyzed as a quality control material (Hill et al., 2016). Intercept ages and initial Pb ratio were calculated using IsoplotR (Vermeesch, 2018). A total of 30 spot analyses were made on the TLM sample.

At IGGCAS, the experiment was performed with an Element XR HR-ICP-MS instrument (Thermo Fisher Scientific, USA) coupled to a 193 nm ArF excimer laser system (Geolas HD, Lambda Physik, Göttingen, Germany). Details on measurement procedures and calibration technique are presented in Wu et al. (2022). A laser spot size of 90 μm, a repetition rate of 10 Hz, and a fluence of ~3.0 J cm^{-2} were used. The Element XR is equipped with a "jet-interface", comprising of a jet sample cone, an X-version skimmer cone and a high capacity vacuum pump (OnTool Booster 150, Asslar, Germany). This leads to a signal enhancement by a factor of 3–5 relative to the standard configuration, resulting in an improved detection capability (Wu et al., 2020). Helium was employed as ablation gas to improve the transport efficiency of ablated aerosols. WC-1 was used as the primary calibration material (Roberts et al., 2017). Duff Brown Tank was analyzed as a quality control material (Hill et al., 2016). The concentrations of U, Th and Pb were reduced using Iolite software with the "Trace_Element" DRS and a semi-quantitative standardization method. NIST SRM 614 was used as the reference material for elemental concentrations and ARM-3 was used for quality control (Wu et al., 2019, 2021). The element concentrations of ARM-3 match with the published data within 20 %.

A second set of U-Pb analyses were carried out at IGGCAS using a Neptune Plus MC-ICP-MS coupled to a Photon Machines Analyte G2 193 nm ArF excimer laser ablation system. A laser spot size of 60 μm, a10 Hz repetition rate and an energy density of ~3.0 J cm^{-2} were used. The details of the measurement procedures and calibration techniques have been presented by Xie et al. (2023). Reference material WC-1 was used as primary calibration material (Roberts et al., 2017) and ASH-15D and JT were analyzed as quality control materials (Guillong et al., 2020; Nuriel et al., 2020). NIST SRM 614 was first used to correct for instrument drift and to correct the isotopic ratio of $^{207}Pb/^{206}Pb$ and $^{238}U/^{206}Pb$, and then the WC-1 was used to correct the matrix bias of the $^{238}U/^{206}Pb$ ratio. Intercept ages and initial Pb ratios were calculated using IsoplotR (Vermeesch, 2018). A total of 39 spot analyses were carried out.

At PP, the experiment was performed using an Element 2 HR-ICP-MS instrument (Thermo Fisher Scientific, USA) coupled to a New Wave Research (ESI) 213 nm laser system. A laser spot size of 100 μm and 10 Hz repetition rate and an energy density of ~3.0 J cm^{-2} were used. WC-1 was used as primary calibration material (Roberts et al., 2017) and Duff Brown Tank was analyzed as a quality control material (Hill et al., 2016). NIST SRM 614 was first used as the reference material to correct for instrument drift and isotopic bias of $^{207}Pb/^{206}Pb$ and $^{238}U/^{206}Pb$, and subsequently WC-1 was used to correct the matrix bias of the $^{238}U/^{206}Pb$ ratio (Roberts et al., 2017). Intercept ages and initial Pb ratios were calculated using IsoplotR (Vermeesch, 2018). A total of 100 spots were analyzed.

At ETH, the experiment was performed using an Element XR HR-ICP-MS instrument (Thermo Fisher Scientific, Germany) coupled to a 193 nm ArF excimer laser ablation system (RESOlution S-155, Australia). Details on measurement procedures and calibration technique can be found in Guillong et al. (2020). NIST SRM 614 was used as reference material to correct for instrument drift and elemental bias of $^{207}Pb/^{206}Pb$ and $^{238}U/^{206}Pb$, and the WC-1 was used to correct the matrix bias of the $^{238}U/^{206}Pb$ ratio. Calcite reference materials RA138, JT, B6 and ASH-15D were analyzed for quality control. The age data of quality control materials are listed in ESI Table S4. Intercept ages and initial Pb ratios were calculated using IsoplotR (Vermeesch, 2018). A total of 49 spot analyses were made and 5 analyses were identified as outliers.

At BGS, U-Pb analyses by LA-ICP-MS utilized a Nu Instruments single-collector Attom ICP-MS, coupled to a New Wave Research (ESI) NWR193UC laser ablation system equipped with a TV2 ablation cell. Laser ablation parameters for carbonates are an 80 μm static spot, ablated for 30 s, at 10 Hz, with a fluence of 3.5–4.0 J cm^{-2}. The depth of the ablation pit using these settings is ca. 35 μm. The details of measurements procedures and calibration technique are presented in Roberts and Walker (2016). Normalization uses a standard-sample bracketing protocol. First, NIST SRM 614 is used for correction of Pb isotope ratios; this is followed by correction of U/Pb ratios using WC-1 calcite. The B6 and ASH-15D calcite reference materials were analyzed for quality control. Data were reduced using Iolite v4 (Paton et al., 2011) and the VizualAge data reduction scheme (Petrus and Kamber, 2012) with further normalization and uncertainty propagation calculated off-line using an in-house Microsoft Excel spreadsheet and following the recommendations for zircon geochronology outlined in Horstwood et al. (2016). A total of 27 spot analyses were made and 1 analysis was identified as an outlier.

3.4. ID-TIMS U-Pb geochronology

U-Pb dating of calcite by ID-TIMS was performed at the GFZ Helmholtz for Geosciences, Potsdam. Sample TLM analyzed here consists of three calcite crystals, which were taken from the same ~30 g batch described earlier.

Calcite fragments were washed in H_2O and acetone before being weighed together with a mixed ^{205}Pb-^{235}U tracer into screw-top Teflon beakers. Samples were dissolved in 2 M HCl and kept on the hotplate at 70 °C overnight. For separation and purification of Pb and U, the dried samples were taken up in 3 M HCl and passed over ion-exchange columns filled with 0.5 mL (1 CV, column volume) AG-1-8× (100–200 mesh) anion exchange resin conditioned with 3 M HCl. The separation procedure includes the following steps: add sample in a few drops 3 M HCl, add 2 CV 3 M HCl, add 8 CV 0.9 M HBr, add 2 CV 2 M HCl, and elute Pb using 6CV 3 M HCl. Uranium was eluted and collected in a separate beaker during the HBr-step. The U fraction was dried to near dryness. Remaining Br-complexes were destroyed by adding a few drops of 7 M HNO_3 and the samples were dried at low temperature. The U fraction was taken up in 7 M HNO_3 and loaded on the same column, conditioned using 7 M HNO_3, earlier used for the separation of Pb. After sample addition, U was purified using 6 CV 7 M HNO_3, 6 CV 6 M HCl, and eluted using 6 CV 0.1 M HCl.

Lead and U were loaded on separate Re single-filaments using H_3PO_4 and silica gel as emitter. Lead and U were measured using a Thermo-Fisher Scientific Triton multi-collector mass-spectrometer operated in static multi-collection using Faraday for ^{208}Pb, ^{207}Pb, ^{206}Pb and ^{205}Pb and an ion counter for ^{204}Pb. Lead data were collected at 1200–1260 °C and U data were collected at 1370–1430 °C. Analytical data were corrected for mass bias using 0.1 % / a.m.u. as determined by the repeated measurement of reference material NBS 981. Total blanks were better than 15 pg for Pb and 1 pg for U. The data were plotted using Isoplot v.3 (Ludwig, 2003).

3.5. Carbon, O and Sr isotope analysis

Carbon and O isotope ratios of TLM were determined using a Thermo Fisher MAT 253 isotope ratio mass spectrometer (IRMS) coupled to a GasBench II at the Laboratory for Stable Isotope Geochemistry, IGGCAS, through production of CO_2 after reaction with phosphoric acid. The

reaction vial was automatically flushed with high-purity (99.999 %) He gas for 10 min at a flow rate of 100 mL min^{-1} to remove atmospheric contaminants including traces of CO_2 and H_2O vapor. The acid digestion was performed in the GasBench II in continuous flow mode, at a temperature of 72.0 ± 0.1 °C and a reaction time of 60 min, through which the generated CO_2 was transferred by the He carrier gas into the mass spectrometer. Standard deviations of $\delta^{13}C$ and $\delta^{18}O$ values were calculated from replicate analyses of an internal laboratory calcite standard, which are better than 0.15 ‰ and 0.20 ‰, respectively. The measured $\delta^{13}C$ and $\delta^{18}O$ values are reported relative to Vienna Pee Dee Belemnite (V-PDB) respectively. Strontium isotope data were previously determined by TIMS, MC-ICP-MS and LA-MC-ICP-MS (Wu et al., 2023).

4. Results

4.1. Cathodoluminescence images

Fig. 2 shows the CL images of five different zones of TLM calcite. In general, the sample is CL homogenous. Some fractures are seen but can be easily avoided during U-Pb analysis, while very few inclusions were observed (Fig. 2).

4.2. Chemical composition of calcite TLM

Table 2 summarizes the chemical composition of calcite TLM determined by LA-ICP-MS and the individual data are listed in ESI Table S1. TLM is characterized by low Mg, Mn and Fe contents with mean values of 816 ± 66 μg g^{-1}, 22.9 ± 2.8 μg g^{-1} and 44.9 ± 35.0 μg g^{-1}, indicating TLM is a relatively high-purity calcite. The Th/U ratio is c. 0.1. TLM is LREE enriched, with a slightly negative Eu anomaly (Fig. 3). The scatter for most REE (ESI Table S1) reflects their low contents close to detection limit and likely does not reflect sample heterogeneity.

4.3. LA-(Q, SF, MC)-ICP-MS U-Pb ages

Four laboratories used SF-ICP-MS instruments (IGGCAS, PP, ETH and BGS). The individual data are listed in ESI Table S3. The ages in Fig. 4 and Fig. 5 are given as "values ± a/b", where "a" is the calculated uncertainty from IsoplotR and "b" is the total uncertainty propagated through with a 2.5 % systematic uncertainty. A total of 17 sessions were performed at IGGCAS using LA-SF-ICP-MS (Fig. 4a), yielding an intercept age of 223.8 ± 0.8 Ma with initial $^{207}Pb/^{206}Pb$ of 0.877 ± 0.020

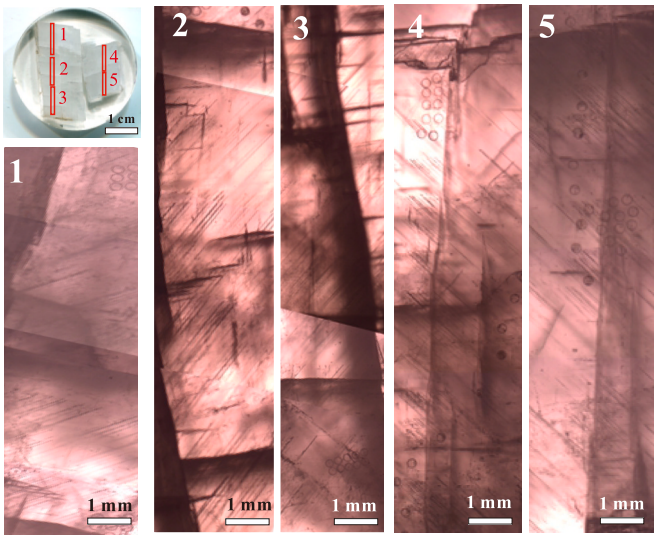

Fig. 2. Cathodoluminescence images of calcite TLM in five different zones.

Table 2
Chemical compositions of TLM determined by LA-ICP-MS.

Element	mass	Mean (μg g^{-1})	2 s	Min (μg g^{-1})	Max (μg g^{-1})
		$n = 26$			
Mg	24	817	66	716	860
Si	29	930	394	608	1343
V	51	0.30	0.20	0.05	0.59
Mn	55	22.9	2.8	21.0	26.0
Fe	57	44.9	35.0	0.55	69
Sr	88	144	36	118	192
Y	89	0.44	0.13	0.34	0.56
Ba	137	0.17	0.27	0.02	0.54
La	139	0.49	0.069	0.43	0.55
Ce	140	1.04	0.15	0.93	1.2
Pr	141	0.13	0.031	0.10	0.15
Nd	143	0.50	0.15	0.36	0.62
Sm	147	0.096	0.074	0.03	0.17
Eu	153	0.019	0.019	0.004	0.043
Gd	158	0.076	0.043	0.036	0.11
Tb	159	0.010	0.009	0.005	0.024
Dy	163	0.063	0.039	0.019	0.10
Ho	165	0.011	0.007	0.003	0.017
Er	166	0.032	0.021	0.015	0.052
Tm	169	0.004	0.004	0.002	0.009
Yb	173	0.029	0.024	0.005	0.059
Lu	175	0.004	0.004	0.0007	0.0083
Pb*		0.021	0.037	0.005	0.077
Th	232	0.043	0.026	0.024	0.090
U	238	0.44	0.58	0.23	1.80

Note:
1. The total Pb contents (Pb*) were calculated using the equation $Pb^* = 0.241 \times Pb^{206}_{Total} + 0.221 \times Pb^{207}_{Total} + 0.524 \times Pb^{208}_{Total}$. All the values are given in μg g^{-1}. Pb^{20X}_{Total} refer to the total Pb concentrations calculated from each isotope using ARM-1 as reference material for standardization. Factors 0.241, 0.221, 0.524 correspond to the natural isotopic abundances of the Pb isotopes. Due to the very low contribution of ^{204}Pb to the total Pb contents, we thus ignore ^{204}Pb.
2. The full data set is reported in ESI table S2.

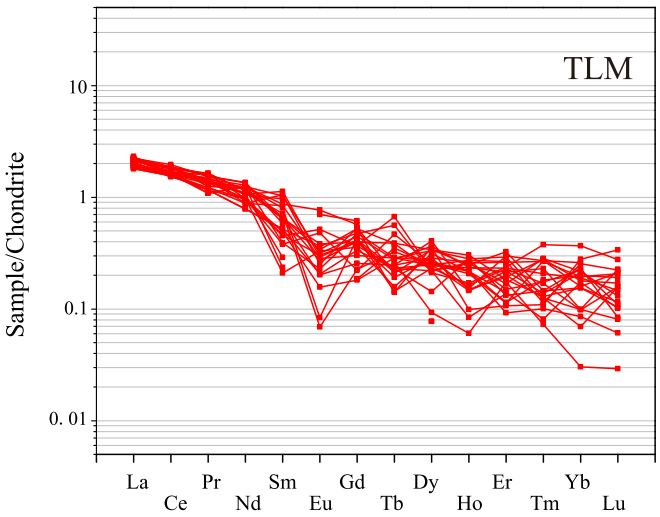

Fig. 3. Rare earth element pattern (normalized to CI chondrite) of calcite TLM determined by LA-ICP-MS. The individual data are listed in ESI Table S2.

and an anchored intercept age of 223.0 ± 0.7 Ma ($^{207}Pb/^{206}Pb$ anchored at 0.838). Seventeen independent sessions at IGGCAS yielded a weighted mean of the intercept ages of 222.6 ± 1.5 Ma (Fig. 4b). A single session with 100 spot analyses was performed at PP using LA-SF-ICP-MS (Fig. 5b), yielding an intercept age of 220.1 ± 2.0 Ma with initial $^{207}Pb/^{206}Pb$ of 0.798 ± 0.087 and an anchored intercept age of 221.0 ± 1.1 Ma ($^{207}Pb/^{206}Pb$ anchored at 0.838). A single session with 44 spot analyses was performed at ETH using LA-SF-ICP-MS (Fig. 5c), yielding an intercept age of 219.6 ± 1.4 Ma with an initial $^{207}Pb/^{206}Pb$ of 0.930

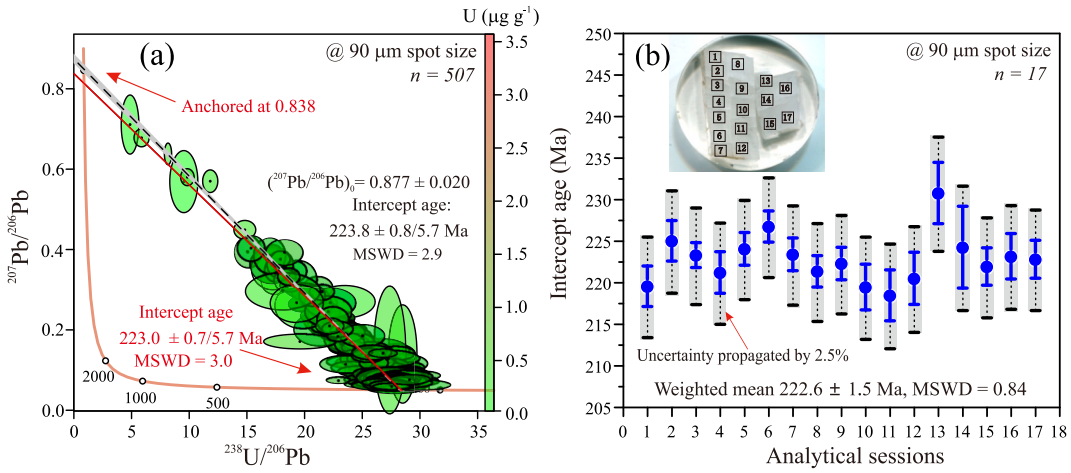

Fig. 4. (a) Tera-Wasserburg U-Pb diagram showing the LA-SF-ICP-MS U-Pb isotope data obtained from IGGCAS. Ellipses are 2σ (SE) calculated from individual spot analysis. The unanchored and anchored ($^{207}Pb/^{206}Pb_i$ at 0.838) ages were calculated. The ages are given as "values ± a/b", where "a" is the uncertainty derived from regression of the data points and "b" is propagated and includes systematic uncertainty (2.5 %). The color of error ellipses is keyed to the U concentrations (color bar on right side of panel). The data are listed in ESI Table S3; (b) Weighted-mean $^{206}Pb/^{238}U$ ages for sample calcite TLM obtained in seventeen sessions. Uncertainty bars are 2σ, with the blue bars representing the uncertainty derived from data point regressions and the dashed black bars those including systematic uncertainties. (For interpretation of the references to color in this figure legend, the reader is referred to the web version of this article.)

± 0.110 and an anchored intercept age of 219.1 ± 1.3 Ma ($^{207}Pb/^{206}Pb$ anchored at 0.838). Five spot analyses were identified as outliers. A single session with 27 spot analyses were performed at BGS using LA-SF-ICP-MS (Fig. 5d), yielding an intercept age of 220.1 ± 1.8 Ma with an initial $^{207}Pb/^{206}Pb$ of 0.870 ± 0.460 and an anchored intercept age of 220.1 ± 1.8 Ma ($^{207}Pb/^{206}Pb$ anchored at 0.838). One analysis was identified as an outlier.

One lab used an LA-MC-ICP-MS setup (IGGCAS). The individual data are listed in ESI Table S3. A single session with 39 spots yielded an intercept age of 224.0 ± 0.8 Ma with an initial $^{207}Pb/^{206}Pb$ of 0.898 ± 0.024 and an anchored intercept age of 223.6 ± 1.0 Ma ($^{207}Pb/^{206}Pb$ anchored at 0.838) (Fig. 5a). Three labs used Q-ICP-MS instruments (TCD, ITRCAS and CAGS). One mapping session at TCD was split in 40 "pseudo-analyses"using $^{207}Pb/^{235}U$ as the pooling channel and gave an intercept age of 223.2 ± 1.6 Ma with an initial $^{207}Pb/^{206}Pb$ of 0.824 ± 0.120 while anchoring to $^{207}Pb/^{206}Pb = 0.838$ results in an intercept age of 223.2 ± 1.4 Ma (Fig. 5e). A single session with 27 spot analyses was performed at ITRCAS and yielded an intercept age of 224.1 ± 2.3 Ma with an initial $^{207}Pb/^{206}Pb$ of 0.860 ± 0.110 and an anchored intercept age of 223.9 ± 1.8 Ma ($^{207}Pb/^{206}Pb$ anchored at 0.838) (Fig. 5f). No data were identified as outliers. A single session with 30 spot analyses was performed at CAGS and yielded an intercept age of 224.4 ± 5.0 Ma with a poorly constrained initial $^{207}Pb/^{206}Pb$ of 0.810 ± 0.520 and an anchored intercept age of 224.6 ± 2.1 Ma ($^{207}Pb/^{206}Pb$ anchored at 0.838) (Fig. 5g). The weighted mean age for the data from eight independent laboratories is 222.3 ± 2.0 Ma (Fig. 5h). Overall, the common Pb in this sample is relatively low and most analyses plot close to the concordia, resulting in a large uncertainty on the $^{207}Pb/^{206}Pb$ intercept values. As shown in Figs. 4 and Fig. 5, some $^{207}Pb/^{206}Pb_{initial}$ values are higher than the corresponding ID values, while others are lower. This discrepancy thus may be related to the large uncertainties on the upper intercept caused by the low common lead content in the sample, along with the potential influence of fluid or other inclusions in the sample. Calcite TLM contains in general low U (mean: 0.35 μg g^{-1}, range: 0.23–1.8 μg g^{-1}) therefore a relatively large spot size is required for LA-ICP-MS analysis.

4.4. ID-TIMS U-Pb ages

Fig. 6 and Table 3 summarize the ID-TIMS results of calcite TLM. Sample TLM has U contents ranging from 0.26 to 0.50 μg g^{-1} and $^{206}Pb/^{204}Pb$ ratios ranging from 21.45 to 116.8 (Table 3). Total Pb contents of most samples are below 0.05 μg g^{-1}. The few analyses with higher Pb contents have higher Pb_{common} contents that vary between 87.2 and 2730 pg Pb (Table 3), i.e., 0.016 and 0.269 μg g^{-1} Pb. These variable contributions of common Pb account for the wide range in $^{238}U/^{206}Pb$ and $^{207}Pb/^{206}Pb$ ratios of 3.80–24.56 and 0.1489–0.7200, respectively. The large spread in $^{238}U/^{206}Pb$ and $^{207}Pb/^{206}Pb$ ratio constrains the discordia robustly on the Tera-Wasserburg concordia. The analyzed 14 aliquots define a discordia that intercepts at an age of 222.5 ± 2.8 Ma and at a $^{207}Pb/^{206}Pb$ of 0.8380 ± 0.0013 (Fig. 6a). The MSWD of 62 shows that there is some excess scatter. In the $^{238}U/^{204}Pb$ vs. $^{206}Pb/^{204}Pb$ diagram, these 14 aliquots define an isochron that corresponds to an age of 223.8 ± 2.4 Ma (MSWD = 3.6) with a $^{206}Pb/^{204}Pb$ intercept of 18.41 ± 0.35 (Fig. 6b).

4.5. Carbon and O stable isotope data

Table 4 summarizes the C and O isotope data of calcite TLM. The three split analyses yielded a mean $\delta^{13}C$ value of −1.48 ± 0.10 ‰ and a mean $\delta^{18}O$ value of −14.1 ± 0.13 ‰. The data indicate the source of calcite TLM is meteoric freshwater.

5. Discussion

5.1. Homogeneity of U-Pb ages

Homogeneity is a fundamental requirement for any reference material, yet it is not an inherent property of the material itself. Instead, homogeneity is specific to the isotopic ratio and scale of the sample being analyzed. The U-Pb age homogeneity of TLM was evaluated in two ways: (a) by a large number of spot analyses ($n = 507$) on two fragments (one of 2.0 cm × 1.0 cm, and the other one 1.0 cm × 1.0 cm) in a single laboratory (IGGCAS); (2) by multiple analyses from different laboratories ($n = 8$, each laboratory used a different fragment). As shown in Fig. 4a, all 507 U-Pb spot data lie on a single mixing line providing a lower intercept age of 223.0 ± 0.7 Ma when anchored using the initial $^{207}Pb/^{206}Pb$ constraint derived from TIMS analyses (0.8380 ± 0.0013, see below). Data from 17 individual sessions located in different zones (Fig. 4b) show consistent age results within analytical uncertainties. These results indicate that calcite TLM has an age that is homogeneous at the level of LA-ICP-MS measurements. To further demonstrate this,

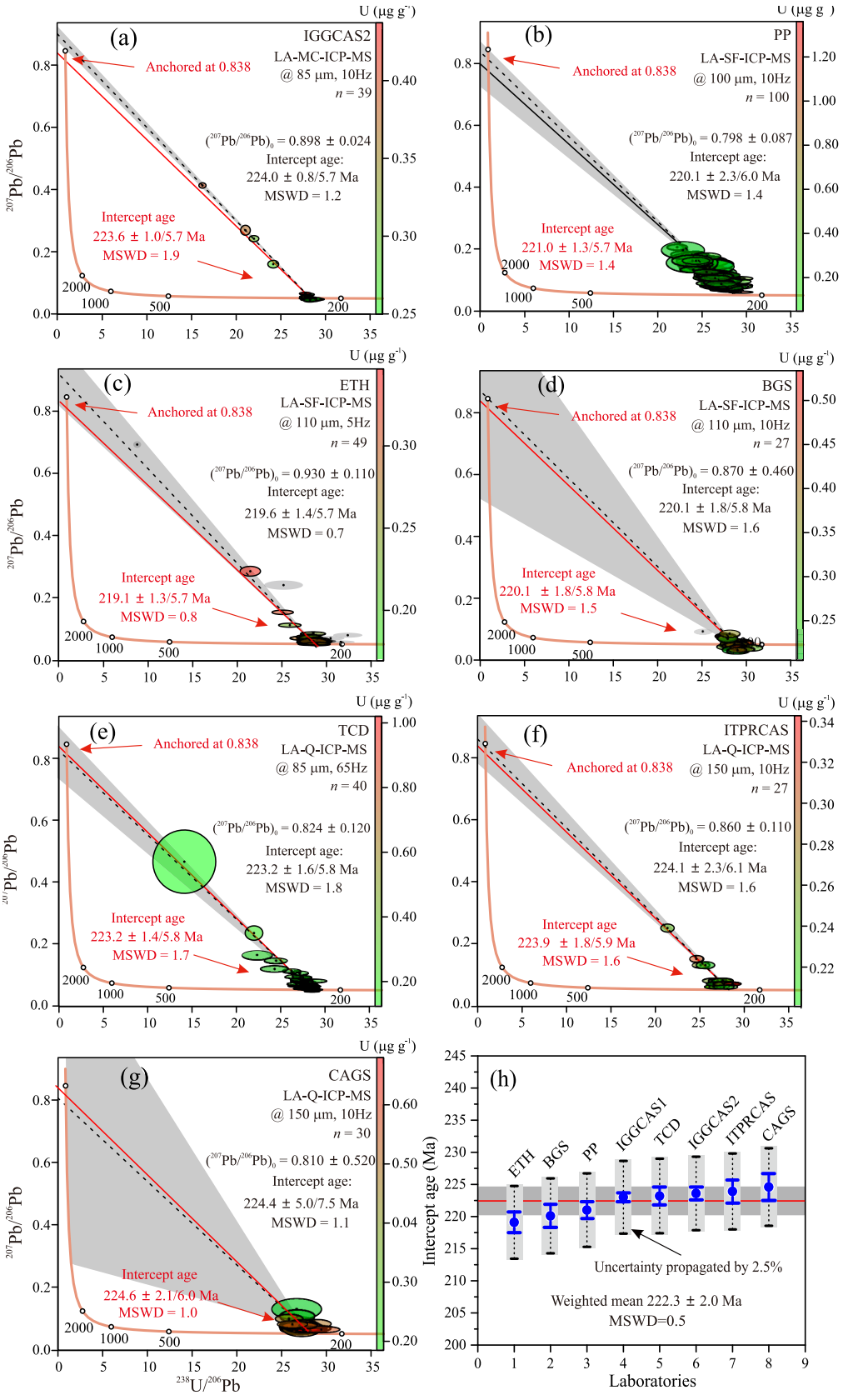

(caption on next page)

Fig. 5. Tera-Wasserburg U-Pb diagram showing the LA-SF-ICP-MS U-Pb isotope data from IGGCAS (a); PP (b); ETH (c); BGI (d); TCD (e); ITPRCAS (f); CAGS (g). Ellipses are 2σ (SE) calculated from individual spot analysis. The unanchored and anchored ($^{207}Pb/^{206}Pb_i$ at 0.838) ages were calculated. The ages are given as "values ± a/b", where "a" is the uncertainty derived from regression of the data points and "b" is propagated and includes systematic uncertainty (2.5 %). The color of error ellipses is keyed to the U concentrations (color bar on right side of panel). Data for the individual analyses are listed in ESI Table S3. Weighted-mean lower intercept ages for sample Calcite TLM obtained in seven laboratories (h). Anchored intercept ages from panels a-g. Uncertainty bars are 2σ, with the blue bars representing the uncertainty derived from data point regressions and the dashed black bars those including systematic uncertainties. The weighted mean and the uncertainty were calculated using the individual uncertainty including systematic uncertainties. (For interpretation of the references to color in this figure legend, the reader is referred to the web version of this article.)

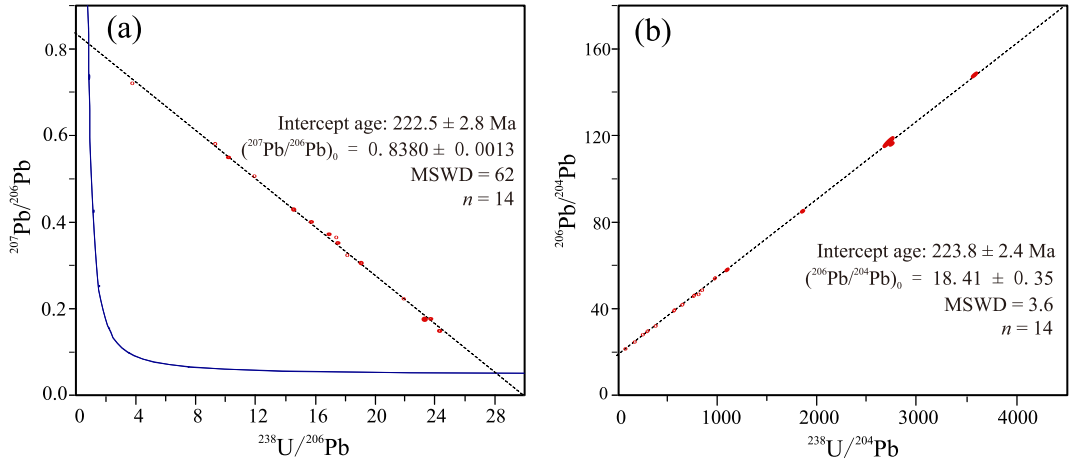

Fig. 6. (a) Tera-Wasserburg concordia diagram showing the ID-TIMS U-Pb intercept age of 222.5 ± 2.8 Ma and the initial $^{207}Pb/^{206}Pb$ value of 0.8380 ± 0.0013. Ellipses are 2σ uncertainties. (b) $^{238}U/^{204}Pb$ vs $^{206}Pb/^{204}Pb$ diagram defining an isochron age of 223.8 ± 2.4 Ma. Ellipses are 2σ uncertainties.

seven other independent laboratories analyzed TLM calcite on different crystal fragments (Fig. 5) yielding consistent data within analytical uncertainties (Fig. 5h).

For the homogeneity evaluation of the individual data, the MSWD values are used. A value smaller than 3 represents a valid isochron in geochronology defined by three criteria (same initial isotopic composition, contemporaneity and a closed system) and indicate the analyzed data represent the same age. We further used the homogeneity index (H) to assess the homogeneity of age data from different sessions and/or laboratories. H represents the ratio of the measurement uncertainty to the expected value of the total combined uncertainty (e.g., Harries, 2014; Batanova et al., 2019). A value of 1 for the index implies that the sample is homogeneous within the analytical uncertainty of individual measurements. A value >3 for the index indicates significant chemical heterogeneity. The H value can be considered as a particular case of an F-test when the degree of freedom of each population approaches infinity. ESI Table S5 lists the Homogeneity indexes that are all smaller than 2, indicating TLM is homogenous across the different analytical sessions and laboratories.

5.2. U concentration and common Pb compositions (f_{206})

Fig. 7 plots the U concentrations and common Pb compositions of calcite TLM. The data are compiled from analytical sessions at IGGCAS using LA-SF-ICP-MS. Calcite TLM contains relatively low U contents with a median value of 0.35 μg g^{-1}, and more than 95 % of the analyses have U contents below 1.0 μg g^{-1} (Fig. 7a). Calcite TLM contains relatively low common Pb. The median common Pb composition (f_{206}) is 4.56 %, and more than 90 % of the analyses yield an f_{206} value below 20 % (Fig. 7b). The low common Pb content is ideal for a primary calcite reference material as it enables primary calibration with a small number of analyses.

5.3. Recommended U-Pb age of TLM and comparisons to other calcite U-Pb reference materials

The ID-TIMS results are the recommended U-Pb age for TLM with a Tera-Wasserburg intercept age of 222.5 ± 2.8 Ma and an initial $^{207}Pb/^{206}Pb$ of 0.8380 ± 0.0013. Table 5 summarizes the currently available calcite U-Pb reference materials, parts of which have ID-TIMS constraints. The ages of these reference materials range from 1.09 Ma to 254 Ma. Among them, WC-1 is widely used as the primary reference material for calcite U-Pb dating, but this material has a relatively large age uncertainty of ~2.5 % which inevitably propagates through to sample unknowns. Recently, a new primary calcite U-Pb reference material (RA138) has been developed (Guillong et al., 2024). This material has relatively high and homogeneous U concentrations (~4 μg g^{-1}, similar to WC-1), and a low U-Pb age uncertainty (~0.2 %, 321.99 ± 0.65 Ma). This material is another choice as primary RM along with WC-1. Other reference materials characterized by ID-TIMS or ID-MC-ICP-MS include Duff Brown Tank, JT, ASH-15D, PTKD-2, TARIM, RioM-1 and SB19.

AXH-1A and TARIM calcites are both from the Tarim Basin, and yield very similar ages (209.8 ± 1.3 Ma and 208.5 ± 0.6 Ma) and similar U concentrations (0.1–0.5 μg g^{-1}), indicating they likely represent the same calcite precipitation event. Calcite TLM also comes from the Tarim Basin, but has an older age (222.5 ± 2.8 Ma) and different Sr content (TLM: ~100 μg g^{-1}, TARIM: ~600 μg g^{-1}) and $^{87}Sr/^{86}Sr$ ratio (TLM: 0.70970, TARIM: 0.71042) (Wu et al., 2023; Li et al., 2025), indicating they have different sources. In summary, calcite TLM has relatively low U concentrations (~0.35 μg g^{-1}), containing a high proportion of radiogenic Pb (common Pb f_{206} < 20 %), and an age uncertainty of ~1.3 %, which makes it suitable for use as a U-Pb primary reference material for low U contents compared to other reference materials, e.g., WC-1 (~ 5 μg g^{-1}), RA138 (~ 4 μg g^{-1}).

5.4. Geological implications

Regional tectonism is primarily represented by conjugate strike-slip

Table 3
ID-TIMS U-Pb isotope data for TLM calcite.

Sample	Weight	U [a]	Pb [b]	Pb_{common}	$^{206}Pb/^{204}Pb$ [c]	$^{207}Pb/^{204}Pb$ [c]	$^{208}Pb/^{204}Pb$ [c]	$^{238}U/^{204}Pb$ [c]	$^{238}U/^{206}Pb$ [d]			$^{207}Pb/^{206}Pb$ [d]			ρ [d]
	[mg]	[μg g^{-1}]	[μg g^{-1}]	pg					Value	± 2SD	± 2SD %	Value	± 2SD	± 2SD %	
TLM-1a	14.017	0.29	0.016	87.2	147.7	21.99	43.39	3627	24.56	0.11	0.45	0.1489	0.0004	0.24	−0.246
TLM-1b	10.622	0.31	0.023	126	84.86	18.92	47.91	1880	22.16	0.11	0.49	0.2230	0.0008	0.36	−0.347
TLM-1c	19.380	0.46	0.027	221	115.9	20.48	42.38	2780	23.98	0.10	0.42	0.1767	0.0008	0.48	−0.392
TLM-1d	14.314	0.50	0.139	1740	27.89	16.19	39.22	263	9.42	0.04	0.41	0.5805	0.0009	0.15	−0.122
TLM-2a	13.083	0.28	0.032	290	48.46	17.08	39.71	859	17.73	0.08	0.43	0.3524	0.0011	0.3	−0.697
TLM-2b	11.505	0.29	0.059	570	32.00	16.19	38.54	387	12.11	0.05	0.39	0.5061	0.0006	0.12	−0.651
TLM-2c	20.382	0.32	0.078	1370	29.47	16.19	39.25	305	10.33	0.05	0.5	0.5493	0.0004	0.07	−0.229
TLM-2d	11.199	0.29	0.027	198	57.92	17.67	39.85	1118	19.31	0.10	0.52	0.3051	0.0018	0.6	−0.500
TLM-2e	18.824	0.39	0.051	714	41.86	16.78	39.67	667	15.93	0.08	0.49	0.4010	0.0006	0.15	−0.243
TLM-3a	10.648	0.33	0.269	2730	21.45	15.45	39.22	81.6	3.80	0.01	0.37	0.7200	0.0004	0.06	−0.319
TLM-4b	12.707	0.26	0.030	267	46.52	16.97	42.34	820	17.62	0.08	0.44	0.3649	0.0012	0.33	−0.747
TLM-3c	5.128	0.33	0.051	201	39.11	16.78	40.66	576	14.73	0.09	0.64	0.4291	0.0020	0.46	−0.561
TLM-3d	12.047	0.41	0.025	129	116.8	20.52	45.26	2750	23.55	0.13	0.57	0.1757	0.0004	0.23	−0.253
TLM-3e	14.795	0.29	0.035	363	45.96	17.10	42.52	787	17.12	0.08	0.47	0.3721	0.0010	0.27	−0.342
Mean		0.34	0.062	643											
2 s		0.14	0.130	1498											

[a] U and Pb concentrations were determined using a mixed ^{205}Pb-^{235}U tracer.
[b] Common Pb contribution corrected for 15 pg blank Pb.
[c] Ratios corrected for mass discrimination of 0.1 % / A.M.U. and blank contributions of 15 pg for Pb ($^{206}Pb/^{204}Pb$ = 17.5, $^{207}Pb/^{204}Pb$ = 15.5; $^{208}Pb/^{204}Pb$ = 37.5) and 1pg U, respectively.
[d] Ratios corrected for mass discrimination and blank; ρ corresponds to the error correlation.

Table 4
Carbon and O stable isotope data for TLM calcite.

Sample	$\delta^{13}C_{V\text{-}PDB}$ ‰	$\delta^{18}O_{V\text{-}PDB}$ ‰
TLM27	−1.53	−14.2
TLM27	−1.47	−14.2
TLM27	−1.43	−14.1

Note: The measured $\delta^{13}C$ and $\delta^{18}O$ values are reported relative to Vienna Pee Dee Belemnite (V-PDB).

fault systems and high-angle strike-slip fault systems. The strike-slip fault systems in the study area likely provided vertical and lateral migration pathways for karst fluids. Controlled by paleotopography, karst fluids moved from north to south via surface runoff and underground rivers, forming multi-phase palaeohydrological systems on the top of the Yijianfang Formation, Lianglitag Formation, and pre-Carboniferous strata, thereby promoting large-scale karst development (Mendez et al., 2020; Tian et al., 2019; Zhang and Cai, 2007). Previous research has indicated that the large-scale karstic caves in Well TS3 are mainly controlled by faulting (e.g., Mendez et al., 2020). These faults facilitated the lateral migration or vertical infiltration of meteoric freshwater along faults, leading to the formation of subsurface and slow-flow karst systems.

The epigenetic karstification of carbonate rocks plays a significant role in the formation of fissure-cavity-type karst reservoirs (Bagni et al., 2022). Previous research has shown that the Tarim Basin experienced multiple episodes of tectonic uplift and subsidence from the latter Ordovician to the Carboniferous, separated by prolonged periods of exposure and erosion (>100 Ma), that eventually resulted in multi-phase, large-scale development of stratigraphically controlled cave-type reservoirs in this region (Zhang and Cai, 2007). The latter Ordovician to the early Silurian and the later Silurian to the middle Devonian have been identified as the most critical time for karst development (Han et al., 2019; Mendez et al., 2020; Tian et al., 2019; You et al., 2023; Zhang et al., 2023b).

The C, O and Sr isotopes of carbonates are commonly used to trace the sources of the fluids that resulted in carbonate precipitation (Veizer et al., 1999; Zhu et al., 2019). The carbon and oxygen isotopes of TLM are depleted in $\delta^{13}C$ and $\delta^{18}O$ relative to the deep hydrothermal fluid (Fig. 8a) and the $\delta^{13}C$ and $\delta^{18}O$ range for the three TLM calcite fragments is very narrow with $\delta^{13}C$ ranging between −1.43 ‰ and − 1.53 ‰ with an average value of −1.48 ‰, and $\delta^{18}O$ ranging from −14.1 ‰ to −14.2 % with an average value of −14.2 ‰ (Table 4). The average Sr isotope ratio of $^{87}Sr/^{86}Sr$ of TLM calcite is 0.70969 ± 0.00023, 0.70970 ± 0.00004 and 0.70971 ± 0.00002 as determined by 216 LA-MC-ICP-MS spots and analysis of 8 aliquots by solution MC-ICP-MS and TIMS, respectively (data from Wu et al., 2023). From the cross plot of $\delta^{13}C$-$\delta^{18}O$ and $\delta^{18}O$-$^{87}Sr/^{86}Sr$ (modified after Zhu et al., 2019 and Veizer et al., 1999), TLM calcite was probably crystallized from meteoric freshwater. The REE spectrum of TLM calcite shows no positive Ce or Eu anomalies, which is typical for calcite formation from meteoric freshwater (Liu et al., 2008; Lv et al., 2021; You et al., 2023; Zhu et al., 2019).

From a petrographic perspective, dolomites in Well S88, TF193, and TS6 frequently exhibit “bay-like” dissolution features (Lv et al., 2021; You et al., 2023). Residual dolomite crystal fragments are observed within calcite cements, while rhombohedral calcite crystals formed through dedolomitization in TS6 contains remnants of dolomite crystals (Lv et al., 2021; You et al., 2023). The presence of dedolomitization thus further indicates that the fluids forming the megacrystalline calcite in karst caves were likely sourced primarily from meteoric water (You et al., 2023). Previous research indicates that the Tahe Oilfield experienced several geological uplift and erosion and karstification processes which led to the large-scale karst formation in the study area mainly during the latter Ordovician to the early Silurian and the later Silurian to the middle Devonian period (Han et al., 2019; Zhang et al., 2023b). Fig. 9 plots the model for the karst development process of Ordovician

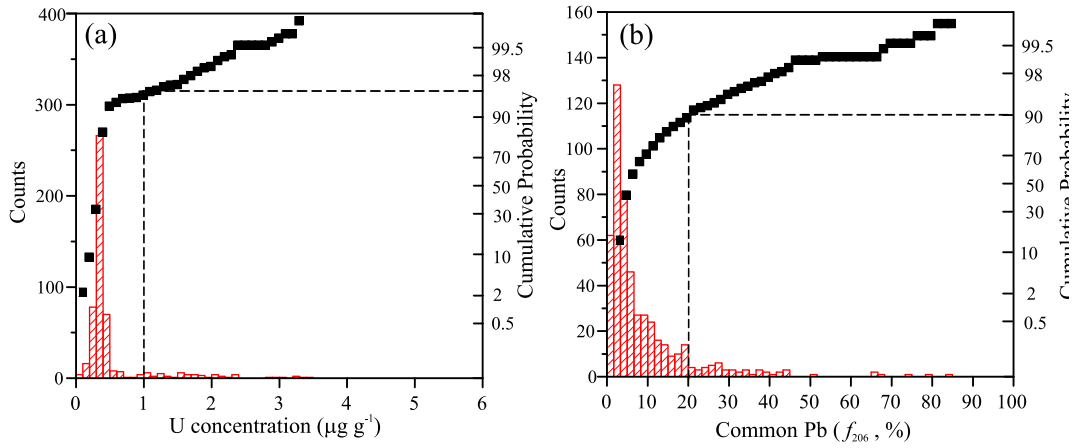

Fig. 7. Cumulative probability and frequency distributions of U concentrations (μg g^{-1}). (b) Cumulative probability and frequency distributions of common Pb (f_{206}, %).

Table 5
Summary of calcite reference materials currently used for U-Pb analysis.

Name	Age (Ma)	2 s	$^{207}Pb/^{206}Pbi$	2 s	U concentration (μg g^{-1})	Characterization method	References
WC-1	254.4	6.4	0.8500	–	~5.0	ID-MC-ICP-MS	Roberts et al., 2017
Duff Brown Tank	64.04	0.67	0.7385	0.0087	5–20	ID-MC-ICP-MS	Hill et al., 2016
JT	13.797	0.031	0.8394	0.0025	~1.0	ID-TIMS	Guillong et al., 2020
ASH-15D	2.965	0.011	0.8306	0.0033	~1.0	ID-TIMS	Nuriel et al., 2020
PTKD-2	153.7	1.7	0.8460	0.0125	~0.16	ID-MC-ICP-MS	Nguyen et al., 2019
TARIM	208.5	0.6	0.8630	0.0060	~0.5	ID-TIMS	Zhang et al., 2023a, 2023b
RA138	321.99	0.65	–	–	~4	ID-MC-ICP-MS	Guillong et al., 2024
RioM-1	63.93	0.11	0.7900	0.0100	~3.7	ID-TIMS	Silva et al., 2025
SB19	1.091	0.006	0.8090	0.0040	3.5	ID-MC-ICP-MS	Wang et al., 2025
AXH-1A	209.8	1.3	–	–	~0.14	LA-ICP-MS	Cheng et al., 2020
AXH-1D	238.23	0.87	0.8660	0.0016	~0.1	LA-ICP-MS	Nguyen et al., 2019
B6	42.99	0.98	–	–	~2.08	LA-ICP-MS	Pagel et al., 2018
LD-5	72.5	1.0	–	–	~0.3	LA-ICP-MS	Kendrick et al., 2022
DC22	153.5	0.8	0.8300	0.0100	~4	LA-ICP-MS	Tang et al., 2025
TLM	222.5	2.8	0.8380	0.0013	~0.35	ID-TIMS	This study

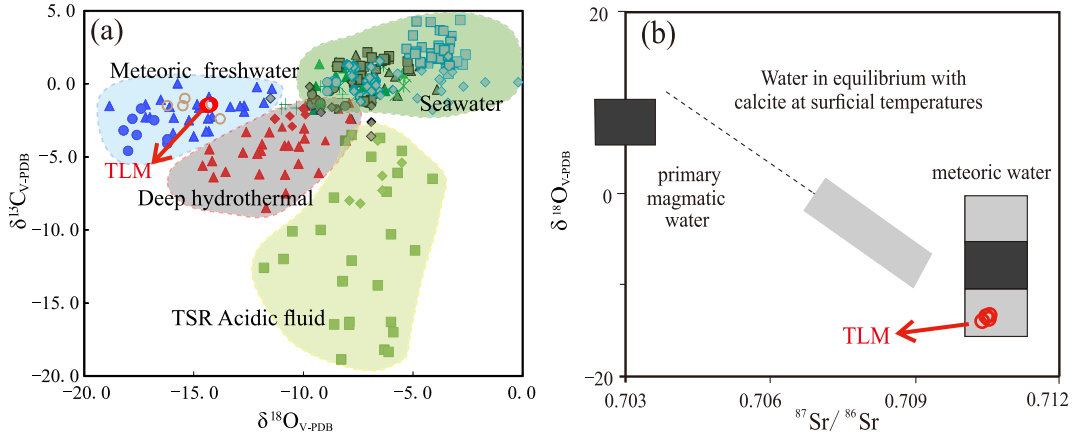

Fig. 8. Carbon, O and Sr isotopic signatures of calcite TLM, indicating that calcite TLM is likely sourced from meteoric water. (a) Ranges of C and O isotopic compositions of different kinds of the carbonate minerals crystallized from different types of fluids in the Tarim, Sichuan and Ordos basins (modified after Zhu et al., 2019). The blue, grey, green and light-green areas represent the carbonate minerals crystallized from the meteoric freshwater, deep hydrothermal water, seawater and TSR Acidic fluids, respectively. The results of TLM's data are shown as red circles. For comparison, data of calcite from the same hole at similar depths is shown as brown circles (Wang et al., 2021). (b) The grey range represents the O and Sr isotopic ranges of Palaeozoic, Mesozoic and Cenozoic samples (modified after Veizer et al., 1999). (For interpretation of the references to color in this figure legend, the reader is referred to the web version of this article.)

Reservoir in Tahe Oilfield. The megacrystalline calcite in the layering controlled giant karst cave in Well TS3 has a well characterized U-Pb age of 222.5 ± 2.8 Ma, indicating that karstification in the studied area may have also occurred in the Triassic (Fig. 9).

Burial history analysis of Well TS3 shows that at c. 222.5 Ma, the burial depth of the Ordovician Yingshan Formation was ~2000 m to ~

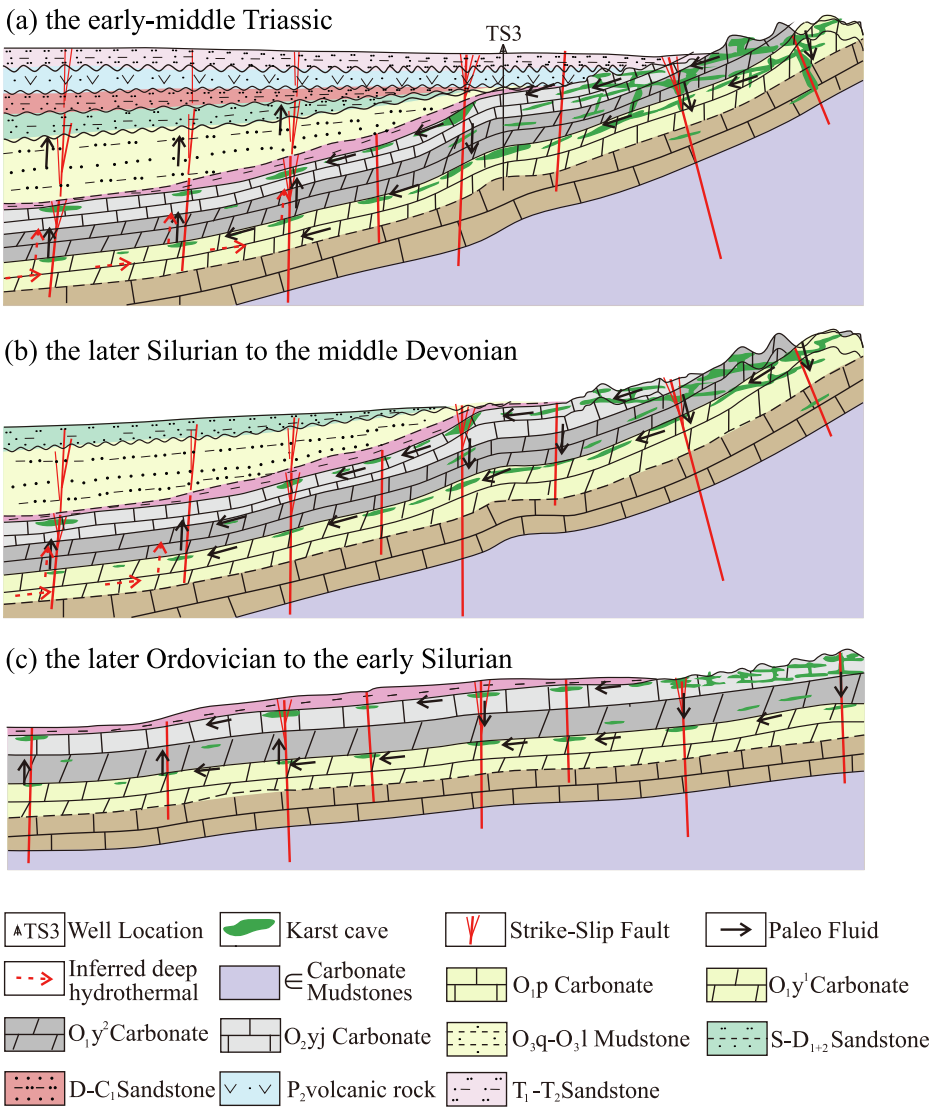

Fig. 9. Model for karst development in the Ordovician Yingshan formation reservoir in the Tahe Oilfield. (a) Karst development during the early-middle Triassic. The meteoric freshwater from the outcrops is transported to deeper layers along the earlier karst system and faults, the karst of the Ordovician Yingshan Formation has further expanded. (b) Karst development after tectonic uplift and erosion in the later Silurian to the middle Devonian. (c) Karst development after tectonic uplift and erosion in the later Ordovician to the early Silurian. Aquitards may have blocked meteoric freshwater flow into deeper layers, favoring the formation of layer-controlled karst.

2700 m (Fig. 9a). It is hypothesized that meteoric freshwater, driven by gravitational forces, differential compaction, and/or osmotic pressure, infiltrated along active strike-slip faults to these depths. Subsequently, this fluid migrated through early karst caves, microfractures, and/or rock pores, spreading laterally along stratigraphic planes within the Yingshan Formation and adjacent layers (Fig. 9). In the TS3 well area, the megacrystalline calcite-filled karst caves were formed by the influences (e.g., precipitation, dissolution) of these fluids (Fig. 9). The combination of calcite U-Pb ages with C, O and Sr isotope data and trace element data provides direct constraints on the source and process of karstification, which are important for the further constraints on the timing of petroleum migration and accumulation in karst host-rocks. Small amounts of calcite TLM reference materials can be obtained on request from the State Key Laboratory of Lithospheric and Environmental Coevolution, Institute of Geology and Geophysics, China Academy of Sciences (email address: shitou.wu@mail.iggcas.ac.cn).

6. Conclusions

A natural calcite sample (TLM) has been characterized and assessed as a new potential reference material for in situ U-Pb geochronology. U-Pb isotopic analyses were conducted across nine different laboratories by isotope dilution TIMS and laser ablation (Q, SF, MC)-ICP-MS, to examine the homogeneity of the TLM calcite crystals. Calcite TLM yields homogeneous LA-ICP-MS ages as indicated by multiple spot analyses from different laboratories. A total of fourteen ID-TIMS analyses yielded an intercept age of 222.5 ± 2.8 Ma with an initial $^{207}Pb/^{206}Pb$ of 0.8380 ± 0.0013. Calcite TLM has relatively low U concentrations (~0.35 μg g^{-1}), commonly shows a high proportion of radiogenic Pb (common Pb f_{206} < 20 %), and has an age uncertainty of ~1.3 %, which makes it suitable for use as a U-Pb primary reference material particularly for calcites with low U contents. The C, O, Sr isotope data and trace element signature indicate that the calcite TLM was likely sourced primarily from meteoric water. The data suggest that recurrent karstification may have affected the study area as late as the Triassic.

CRediT authorship contribution statement

Tianyi Li: Writing – review & editing, Writing – original draft, Software, Resources, Methodology, Investigation, Formal analysis, Data curation. **Ranran Chen:** Writing – review & editing, Writing – original draft, Validation, Software, Resources, Methodology, Investigation, Formal analysis, Data curation. **Shitou Wu:** Writing – review & editing, Writing – original draft, Supervision, Project administration, Methodology, Funding acquisition, Data curation, Conceptualization. **Rolf L. Romer:** Writing – review & editing, Validation, Resources, Methodology, Investigation, Formal analysis, Data curation, Conceptualization. **Nick M.W. Roberts:** Writing – review & editing, Validation, Resources, Investigation, Formal analysis, Data curation. **Kerstin Drost:** Writing – review & editing, Validation, Resources, Investigation, Formal analysis, Data curation. **David Chew:** Writing – review & editing, Visualization, Validation, Resources, Investigation, Formal analysis, Data curation. **Marcel Guillong:** Visualization, Validation, Methodology, Investigation, Formal analysis, Data curation. **Qian Ma:** Visualization, Validation, Investigation, Formal analysis, Data curation. **Yahui Yue:** Visualization, Validation, Methodology, Investigation, Formal analysis, Data curation. **Shuangjian Li:** Resources, Investigation. **Bohang Xie:** Visualization, Validation, Methodology, Investigation, Formal analysis, Data curation. **Ahmatjan Abdurahman:** Resources, Investigation. **Hao Wang:** Writing – review & editing, Visualization, Validation, Methodology, Investigation, Formal analysis, Data curation. **Huixi Lin:** Resources, Investigation. **Yueheng Yang:** Writing – review & editing, Visualization, Validation, Methodology, Investigation, Formal analysis, Data curation. **Xusheng Guo:** Writing – review & editing, Project administration, Conceptualization.

Declaration of competing interest

The authors declare that they have no known competing financial interests or personal relationships that could have appeared to influence the work reported in this paper.

Acknowledgements

We thank Lei Xu, Chao Huang, Liewen Xie and Hongwei Li for their help with sample preparation and analysis. Many thanks to Professor Guo Xiaowen for providing the sample. This work was supported by the National Natural Science Foundation of China (Nos. 42522302, 42273034), the Youth Innovation Promotion Association of the Chinese Academy of Sciences (No 2022066), the Joint Funds for Innovation and Development of Private Enterprises of the National Natural Science Foundation of China (No. U24B6002), the Key Research Program of the Institute of Geology & Geophysics, Chinese Academy of Science (No. IGGCAS-202204), and the Strategy Priority Research Program (Category B) of Chinese Academy of Sciences (No. XDB0710000). KD and DC acknowledge support from Research Ireland through research grant 13/RC/2092_P2 (iCRAG research center). We would like to thank Sonja Aulbach for the editorial handling and two anonymous reviewers for their helpful and constructive comments.

Appendix A. Supplementary data

Supplementary data to this article can be found online at https://doi.org/10.1016/j.chemgeo.2025.123230.

Data availability

No data was used for the research described in the article.

References

Bagni, F.L., Erthal, M.M., Tonietto, S.N., Maia, R.P., Bezerra, F.H., Balsamo, F., Córdoba, V.C., de Souza, F.G., Brod, J.A., Fernandes, C.P., 2022. Karstified layers and caves formed by superposed epigenic dissolution along subaerial unconformities in carbonate rocks–Impact on reservoir-scale permeability. Mar. Pet. Geol. 138, 105523.

Batanova, V., Thompson, J., Danyushevsky, L., Portnyagin, M., Garbe-Schonberg, D., Hauri, E., Kimura, J., Chang, Q., Senda, R., Goemann, K., Chauvel, C., Campillo, S., Ionov, D., Sobolev, A., 2019. New olivine reference material for in situ microanalysis. Geostand. Geoanal. Res. 43, 453–473.

Cheng, T., Zhao, J., Feng, Y., Pan, W., Liu, D., 2020. In-situ LA-MC-ICP-MS U-Pb dating method for low-uranium carbonate minerals. Chin. Sci. Bull. 65 (2–3), 150–154.

Chew, D., Petrus, J., Kamber, B., 2014. U–Pb LA–ICPMS dating using accessory mineral standards with variable common Pb. Chem. Geol. 363, 185–199.

Coogan, L.A., Parrish, R.R., Roberts, N.M.W., 2016. Early hydrothermal carbon uptake by the upper oceanic crust: Insight from in situ U-Pb dating. Geology 44 (2), 147–150.

Drost, K., Chew, D., Petrus, J.A., Scholze, F., Woodhead, J.D., Schneider, J.W., Harper, D. A., 2018. An image mapping approach to U-Pb LA-ICP-MS carbonate dating and applications to direct dating of carbonate sedimentation. Geochem. Geophys. Geosyst. 19 (12), 4631–4648.

Gui, L., Lu, X., Wang, F., Ge, C., Jiang, L., Liu, S., Xie, W., Chen, W., Fan, J., Wu, H., 2025. An improved U-Pb dating method for carbonates via LA-SF-ICP-MS mapping and its applications. Sci. China Earth Sci. 1–16.

Guillong, M., Wotzlaw, J.F., Looser, N., Laurent, O., 2020. Evaluating the reliability of U–Pb laser ablation inductively coupled plasma mass spectrometry (LA-ICP-MS) carbonate geochronology: matrix issues and a potential calcite validation reference material. Geochronology 2 (1), 155–167.

Guillong, M., Samankassou, E., Müller, I.A., Szymanowski, D., Looser, N., Tavazzani, L., Merino-Tomé, Ó., Bahamonde, J.R., Buret, Y., Ovtcharova, M., 2024. RA138 calcite U–Pb LA-ICP-MS primary reference material. Geochronology 6 (3), 465–474.

Han, C., Lin, C., Lu, X., Tian, J., Ren, L., Ma, C., 2019. Petrological and geochemical constraints on fluid types and formation mechanisms of the Ordovician carbonate reservoirs in Tahe Oilfield, Tarim Basin, NW China. J. Pet. Sci. Eng. 178, 106–120.

Hansman, R.J., Albert, R., Gerdes, A., Ring, U., 2018. Absolute ages of multiple generations of brittle structures by U-Pb dating of calcite. Geology 46 (3).

Harries, D., 2014. Homogeneity testing of microanalytical reference materials by electron probe microanalysis (EPMA). Chem. Erde Geochem. 74, 375–384.

Hill, C.A., Polyak, V.J., Asmerom, Y., Provencio, P., 2016. Constraints on a late cretaceous uplift, denudation, and incision of the Grand Canyon region, southwestern Colorado Plateau, USA, from U-Pb dating of lacustrine limestone. Tectonics 35 (4), 896–906.

Hoareau, G., Claverie, F., Pecheyran, C., Paroissin, C., Grignard, P.A., Motte, G., Chailan, O., Girard, J.P., 2021. Direct U–Pb dating of carbonates from micron-scale femtosecond laser ablation inductively coupled plasma mass spectrometry images using robust regression. Geochronology 3 (1), 67–87.

Horstwood, M.S., Košler, J., Gehrels, G., Jackson, S.E., McLean, N.M., Paton, C., Pearson, N.J., Sircombe, K., Sylvester, P., Vermeesch, P., 2016. Community-derived standards for LA-ICP-MS U-(Th-) Pb geochronology–uncertainty propagation, age interpretation and data reporting. Geostand. Geoanal. Res. 40 (3), 311–332.

Jochum, K.P., Willbold, M., Raczek, I., Stoll, B., Herwig, K., 2005. Chemical characterisation of the USGS reference glasses GSA-1G, GSC-1G, GSD-1G, GSE-1G, BCR-2G, BHVO-2G and BIR-1G using EPMA, ID-TIMS, ID-ICP-MS and LA-ICP-MS. Geostand. Geoanal. Res. 29 (3), 285–302.

Jochum, K.P., Weis, U., Stoll, B., Kuzmin, D., Yang, Q.C., Raczek, I., Jacob, D.E., Stracke, A., Birbaum, K., Frick, D.A., Günther, D., Enzweiler, J., 2011. Determination of reference values for NIST SRM 610-617 glasses following ISO guidelines. Geostand. Geoanal. Res. 35 (4), 397–429.

Kendrick, M.A., Plümper, O., Zhao, J.-X., Feng, Y., Defliese, W.F., Müller, I.A., Ziegler, M., 2022. Exhumation and carbonation of the Atlantis Bank core complex constrained by in situ U-Pb dating and Δ47 thermometry of calcite veins, SW Indian Ridge. Earth Planet. Sci. Lett. 584, 117474.

Li, Q., Parrish, R.R., Horstwood, M.S.A., McArthur, J.M., 2014. U–Pb dating of cements in Mesozoic ammonites. Chem. Geol. 376, 76–83.

Li, H.-J., Hu, Z.-Z., Zhang, L.-L., Zhu, D.-C., Xie, J.-C., Wang, Q., Xu, W.-T., Xu, L.-J., Guo, W., Wu, J., 2025. Two potential natural calcite reference materials for laser in situ Sr isotope analysis. J. Anal. At. Spectrom. 40 (9), 2296–2305.

Liu, C., Li, G., Zhu, C., Liu, G., Lu, Y., 2008. Geochemistry characteristics of carbon, oxygen and strontium isotopes of calcites filled in karstic fissure-cave in Lower-Middle Ordovician of Tahe Oilfield, Tarim Basin. Earth Sci. J. China Univ. Geosci. 33 (3), 377–386.

Ludwig, K., 2003. ISOPLOT 3.00: A Geochronology Toolkit for Microsoft Excel, 70. Berkeley Geochronological Center Special Publication, Berkeley, pp. 1–70.

Lv, Y., Lv, J., Xu, X., Deng, G., Liu, Y., Liu, C., Zhang, Z., Han, Y., 2021. Genetic mechanism of inner reservoirs of Yingshan formation of middle-lower Ordovician in Tahe oil field, Tarim Basin. Pet. Geol. Exp. 43 (6), 1031–1037.

Mason, A.J., Henderson, G.M., Vaks, A., 2013. An acetic acid-based extraction protocol for the recovery of U, Th and Pb from calcium carbonates for U-(Th)-Pb geochronology. Geostand. Geoanal. Res. 37 (3), 261–275.

Mendez, J.N., Jin, Q., González, M., Zhang, X., Lobo, C., Boateng, C.D., Zambrano, M., 2020. Fracture characterization and modeling of karsted carbonate reservoirs: A case study in Tahe oilfield, Tarim Basin (western China). Mar. Pet. Geol. 112, 104104.

Moorbath, S., Taylor, P., Orpen, J., Treloar, P., Wilson, J., 1987. First direct radiometric dating of Archaean stromatolitic limestone. Nature 326 (6116), 865–867.

Nguyen, A., Cheng, T., Woodhead, J., Caulfield, J., Zhao, J.-X., 2019. LA-(MC)-ICPMS U-Pb Geochronology: Potential Calcite Reference Materials. Goldschmidt Barc.
Nuriel, P., Wotzlaw, J.-F., Ovtcharova, M., Vaks, A., Stremtan, C., Šala, M., Roberts, N. M., Kylander-Clark, A.R., 2020. The use of ASH-15 flowstone as a matrix-matched reference material for laser-ablation U-Pb geochronology of calcite. Geochronology 3, 35–47.
Pagel, M., Bonifacie, M., Schneider, D.A., Gautheron, C., Brigaud, B., Calmels, D., Cros, A., Saint-Bezar, B., Landrein, P., Sutcliffe, C., 2018. Improving paleohydrological and diagenetic reconstructions in calcite veins and breccia of a sedimentary basin by combining Δ47 temperature, δ18Owater and U-Pb age. Chem. Geol. 481, 1–17.
Paton, C., Hellstrom, J., Paul, B., Woodhead, J., Hergt, J., 2011. Iolite: Freeware for the visualisation and processing of mass spectrometric data. J. Anal. At. Spectrom. 26 (12), 2508–2518.
Petrus, J.A., Kamber, B.S., 2012. VizualAge: a novel approach to laser ablation ICP-MS U-Pb geochronology data reduction. Geostand. Geoanal. Res. 36 (3), 247–270.
Petrus, J., Chew, D., Leybourne, M., Kamber, B., 2017. A new approach to laser-ablation inductively-coupled-plasma mass-spectrometry (LA-ICP-MS) using the flexible map interrogation tool 'Monocle'. Chem. Geol. 463, 76–93.
Rasbury, E.T., Cole, J.M., 2009. Directly dating geologic events: U-Pb dating of carbonates. Rev. Geophys. 47 (3), 1–27.
Ring, U., Gerdes, A., 2016. Kinematics of the Alpenrhein-Bodensee graben system in the Central Alps: Oligocene/Miocene transtension due to formation of the Western Alps arc. Tectonics 35 (6), 1367–1391.
Roberts, N.M.W., Walker, R.J., 2016. U-Pb geochronology of calcite-mineralized faults: absolute timing of rift-related fault events on the Northeast Atlantic margin. Geology 44 (7), 531–534.
Roberts, N.M.W., Rasbury, E.T., Parrish, R.R., Smith, C.J., Horstwood, M.S.A., Condon, D.J., 2017. A calcite reference material for LA-ICP-MS U-Pb geochronology. Geochem. Geophys. Geosyst. 18 (7), 2807–2814.
Roberts, N.M.W., Drost, K., Horstwood, M.S.A., Condon, D.J., Chew, D., Drake, H., Milodowski, A.E., McLean, N.M., Smye, A.J., Walker, R.J., Haslam, R., Hodson, K., Imber, J., Beaudoin, N., Lee, J.K., 2020. Laser ablation inductively coupled plasma mass spectrometry (LA-ICP-MS) U–Pb carbonate geochronology: strategies, progress, and limitations. Geochronology 2 (1), 33–61.
Silva, M., Lana, C., Scholz, R., Buick, I., Kamo, S., Roberts, N.M.W., Gerdes, A., Wiedenbeck, M., Schoene, B., Apen, F.E., Gaynor, S.P., 2025. RioM-1: a new calcite reference material for U-Pb LA-ICP-MS geochronology. Geostand. Geoanal. Res. https://doi.org/10.1111/ggr.70018.
Smith, P., Farquhar, R., Hancock, R., 1991. Direct radiometric age determination of carbonate diagenesis using U-Pb in secondary calcite. Earth Planet. Sci. Lett. 105 (4), 474–491.
Tang, Y.-W., Liu, N., Han, J.-J., Liu, Y., Ge, W.-T., Gao, J.-F., Lan, T.-G., 2025. Fs–LA–ICP–MS U–Pb dating of fluorite and its prospect for geological application. Chem. Geol. 695, 123083.
Tian, F., Di, Q., Jin, Q., Cheng, F., Zhang, W., Lin, L., Wang, Y., Yang, D., Niu, C., Li, Y., 2019. Multiscale geological-geophysical characterization of the epigenic origin and deeply buried paleokarst system in Tahe Oilfield, Tarim Basin. Mar. Pet. Geol. 102, 16–32.
Veizer, J., Ala, D., Azmy, K., Bruckschen, P., Buhl, D., Bruhn, F., Carden, G.A., Diener, A., Ebneth, S., Godderis, Y., 1999. $^{87}Sr/^{86}Sr$, $\delta^{13}C$ and $\delta^{18}O$ evolution of Phanerozoic seawater. Chem. Geol. 161 (1–3), 59–88.
Vermeesch, P., 2018. IsoplotR: A free and open toolbox for geochronology. Geosci. Front. 9 (5), 1479–1493.
Wang, J., Kang, L., Niu, X., Zhang, H., Li, Y., Zhao, J., Chen, R., Woodhead, J., Zhang, L.-L., Wu, S., Liang, F., Jia, X., Dong, X., Ning, Y., Cheng, H., 2025. An astronomically validated U–Pb reference material for dating Quaternary speleothems. J. Anal. At. 40, 3403–3412.
Wang, B., Yang, Y., Cao, Z., He, S., Zhao, Y., Guo, X., Liu, Y., Chen, J., Zhao, J.-X., 2021. U-Pb Dating of Calcite Veins Developed in the Middle-Lower Ordovician Reservoirs in Tahe Oilfield and Its Petroleum Geologic Significance in Tahe Oilfield. Journal of Earth Science 46 (9), 3203–3216.
Woodhead, J., Pickering, R., 2012. Beyond 500ka: Progress and prospects in the UPb chronology of speleothems, and their application to studies in palaeoclimate, human evolution, biodiversity and tectonics. Chem. Geol. 322-323, 290–299.
Woodhead, J., Hellstrom, J., Maas, R., Drysdale, R., Zanchetta, G., Devine, P., Taylor, E., 2006. U–Pb geochronology of speleothems by MC-ICPMS. Quat. Geochronol. 1 (3), 208–221.
Wu, S., Karius, V., Schmidt, B.C., Simon, K., Wörner, G., 2018. Comparison of ultrafine powder pellet and flux-free fusion glass for bulk analysis of granitoids by laser ablation-inductively coupled plasma-mass spectrometry. Geostand. Geoanal. Res. 42 (4), 575–591.
Wu, S., Wörner, G., Jochum, K.P., Stoll, B., Simon, K., Kronz, A., 2019. The preparation and preliminary characterisation of three synthetic andesite reference glass materials (ARM-1, ARM-2, ARM-3) for in situ microanalysis. Geostand. Geoanal. Res. 43 (4), 567–584.
Wu, S., Yang, M., Yang, Y., Xie, L., Huang, C., Wang, H., Yang, J., 2020. Improved in situ zircon U–Pb dating at high spatial resolution (5–16 μm) by laser ablation–single collector–sector field–ICP–MS using Jet sample and X skimmer cones. Int. J. Mass Spectrom. 456, 116394.
Wu, S., Yang, Y., Jochum, K.P., Romer, R.L., Glodny, J., Savov, I.P., Agostini, S., De Hoog, J.C.M., Peters, S.T.M., Kronz, A., Zhang, C., Bao, Z., Wang, X., Li, Y., Tang, G., Feng, L., Yu, H., Li, Z., Le, Z., Lin, J., Zeng, Y., Xu, C., Wang, Y., Cui, Z., Deng, L., Xiao, J., Liu, Y., Xue, D., Di, Z., Jia, L., Wang, H., Xu, L., Huang, C., Xie, L., Pack, A., Wörner, G., He, M., Li, C., Yuan, H., Huang, F., Li, Q., Yang, J., Li, X., Wu, F., 2021. Isotopic compositions (Li-B-Si-O-Mg-Sr-Nd-Hf-Pb) and Fe2+/ΣFe ratios of three synthetic andesite glass reference materials (ARM-1, ARM-2, ARM-3). Geostand. Geoanal. Res. 45 (4), 719–745.
Wu, S., Yang, Y., Roberts, N.M.W., Yang, M., Wang, H., Lan, Z., Xie, B., Li, T., Xu, L., Huang, C., Xie, L., Yang, J., Wu, F., 2022. In situ calcite U−Pb geochronology by high-sensitivity single-collector LA-SF-ICP-MS. Sci. China Earth Sci. 65 (6), 1146–1160.
Wu, S., Yang, Y., Li, T., Huang, C., Bao, Z., Li, Y., Li, C., Xu, L., Wang, H., Xie, L., 2023. Calcite TLM and LSJ07–two natural low-Sr reference materials for microbeam Sr isotope analysis. J. Anal. At. Spectrom. 38 (12), 2528–2537.
Xie, B., Wu, S., Yang, Y., Wang, H., Zhao, Z., Huang, C., Xie, L., 2023. LA-MC-ICP-MS calcite U-Pb dating technique. Acta Petrol. Sin. 39 (1), 236–248 (In Chinese with English abstract).
Yokoyama, T., Kimura, J.-I., Mitsuguchi, T., Danhara, T., Hirata, T., Sakata, S., Iwano, H., Maruyama, S., Chang, Q., Miyazaki, T., Murakami, H., Saito-Kokubu, Y., 2018. U-Pb dating of calcite using LA-ICP-MS: Instrumental setup for non-matrix-matched age dating and determination of analytical areas using elemental imaging. Geochem. J. 52 (6), 531–540.
You, D., Peng, S., He, Z., Liu, Y., Han, J., Xiao, C., Li, Y., 2023. Scope and mechanism of deep fluid circulation in karst systems, northern Awati-Manjiaer transition zone, Tarim Basin. Earth Sci. Front. 30 (6), 69.
Zhang, T., Cai, X., 2007. Caledonian paleo-karstification and its characteristics in Tahe area, Tarim Basin. Acta Geol. Sin. 81 (8), 1125–1134.
Zhang, L.-L., Zhu, D.-C., Yang, Y.-H., Wang, Q., Xie, J.-C., Zhao, Z.-D., 2021. U-Pb geochronology of carbonate by laser ablation MC-ICPMS: method improvements and geological applications. At. Spectrosc. 42 (6), 335–348.
Zhang, L.-L., Zhu, D.-C., Xie, J.-C., Wang, Q., Kamo, S., Rochin-Banaga, H., Xiao, Y., 2023a. TARIM Calcite: A potential reference material by Laser ICPMS in situ calcite U–Pb dating. J. Anal. At. Spectrom. 38, 2302–2312.
Zhang, H., Cai, Z., Hao, F., Hu, W., Lu, X., Wang, Y., 2023b. Hypogenic origin of paleocaves in the Ordovician carbonates of the southern Tahe oilfield, Tarim basin, Northwest China. Geoenergy Sci. Eng. 225, 211669.
Zhu, D., Liu, Q., Zhang, J., Ding, Q., He, Z., Zhang, X., 2019. Types of fluid alteration and developing mechanism of deep marine carbonate reservoirs. Geofluids 2019 (1), 3630915.